buildings

MDPI

Article

End-One-Flange Web Crippling Behavior of Cold-Formed High-Strength Steel Channels with Web Holes at Elevated Temperatures

Zhiyuan Fang [1,2], Krishanu Roy [1,*], Dinesh Lakshmanan Chandramohan [1], Amirmohammad Yousefi [3], Yazeed Al-Radhi [2] and James B. P. Lim [1,2]

[1] School of Engineering, The University of Waikato, Hamilton 3240, New Zealand
[2] Department of Civil and Environmental Engineering, The University of Auckland, Auckland 1010, New Zealand
[3] School of Engineering, Design and Built Environment, Western Sydney University, Penrith, NSW 2751, Australia
* Correspondence: krishanu.roy@waikato.ac.nz

Abstract: This paper investigates the web crippling strength of cold-formed high-strength steel (CHS) channels with centered web holes subjected to end-one-flange (EOF) loading at elevated temperatures, considering both flanges fastened and unfastened to load plates conditions. The stress-strain curve and material properties for CHS (S690QL steel grade) channels were adopted from the literature, where the temperatures ranged from 20 to 800 °C. The material characteristics were incorporated into finite element (FE) models using ABAQUS. The developed FE model was then validated against the published test results to evaluate the effects of various parameters including web hole diameter, bearing length, cross-section sizes, and flange fastening conditions of such channels at elevated temperatures, and a comprehensive parametric investigation including a total of 1710 validated finite element models was performed. From the parametric study results, it was found that the web crippling strength reduction factor is sensitive to the changes of the hole size and the bearing length, with the parameters of hole size having the largest effect on the web crippling reduction factor; however, the web crippling strength reduction factor remains stable when the temperature is changed from 20 to 800 °C. According to the FEA results, new reliable web crippling strength reduction factor equations for such CHS channels were proposed. In the comparison of proposed design strengths to the numerical failure load, the proposed design equations are suitable to predict the web crippling strength for CHS channels subject to EOF loading at ambient and elevated temperatures.

Keywords: web crippling; numerical simulation; end-one-flange; proposed equation; elevated temperature; high-strength steel

Citation: Fang, Z.; Roy, K.; Chandramohan, D.L.; Yousefi, A.; Al-Radhi, Y.; Lim, J.B.P. End-One-Flange Web Crippling Behavior of Cold-Formed High-Strength Steel Channels with Web Holes at Elevated Temperatures. *Buildings* **2023**, *13*, 266. https://doi.org/10.3390/buildings13020266

Academic Editors: Paulo Santos and Harry Far

Received: 29 November 2022
Revised: 6 January 2023
Accepted: 12 January 2023
Published: 17 January 2023

1. Introduction

Cold-formed high-strength steel (CHS) channel section is a common solution for steel structures requiring higher capacity than typical cold-formed steel sections. The superior quality of CHS channel enables the members to retain higher strength while weighing less than conventional hot-rolled steel. Due to these advantages, CHS channel members are often used in beams, columns, wall panels, and cladding systems. However, when CHS members are considered for building construction, localized web failure and fire safety are two major concerns. This study will investigate the effects of elevated temperatures on the web crippling strength of CHS channels with web holes under EOF loading.

Several studies focused on how cold-formed steel (CFS) structures react when exposed to high temperatures [1–6]. The mechanical characteristics of low and high-strength CFS sections at elevated temperatures were studied experimentally [1–3]. Javed et al. [4] have conducted a review study on the effects of fire loading on the CFS beams and columns, discussing the strength and failure mechanism of such members. In other studies, Fang et al. [5,6] performed numerical simulations on CFS members subjected to web

crippling and axial compression. Gunalan et al. [7] studied the compressive behavior of lipped and unlipped CFS channels at high temperatures. However, none of the abovementioned research studies addressed the web crippling performance of cold-formed structural members, including CHS perforated channels at fire loading.

In the literature, Chan and Young [8] investigated the web crippling strength of CFS beams with stiffening lips at high temperatures. They compared the findings from FE modelling against the calculated capacities determined from the Direct Strength Method (DSM) and Effective Width Method (EWM). Gunalan et al. [9] conducted a numerical simulation on CFS column members under fire loading and studied their flexural-torsional buckling behavior. It was found that for moment released columns under flexural-torsional buckling, lower mechanical properties exhibited high agreement and consistency [9]. In addition, the results from FE models were compared against design guidelines from Australia/New Zealand Standard 4600 (AS/NZS) [10], BS 5950 Part 5 [11], Eurocode 3 Parts 1.2 [12] and 1.3 [13], and DSM [9]. In other research, Gunalan et al. [7] recently determined that using non-linear stress-strain parameters in the CFS might improve the accuracy level of proposed design recommendations in the available design standards.

Furthermore, Rokilan and Mahendran [14] conducted a research study to consider the impacts of material characteristics of the sections at elevated temperatures to further investigate the veracity of these findings. According to their findings, the design equations of EWM and DSM offered both conservative and unconservative estimations for determining the capacity of CFS members under various steel mechanical properties. In addition, they proposed a strength reduction factor for low and high steel sections exhibiting high temperatures up to 700 °C.

In terms of web crippling studies at room/ambient temperature, Uzzaman et al. [15–22] used experimental and numerical simulation to study the web crippling strength of CFS perforated channel beams. Janarthanan et al. [23,24] studied the web crippling strength and failures of CFS channels, and they proposed modified coefficients to estimate the failure load. Gunalan and Mahendran [25] conducted experimental tests to study the web crippling strength of CFS channel sections and proposed design equations within the Direct Strength Method guidelines [10,26]. These studies investigated mainly the cold-formed low-strength steel channels. However, the web crippling strength of cold-formed structural members (e.g., CHS channels) under EOF loading at high temperatures was not taken into account.

Thus, this research aims to investigate the web crippling strength of CHS channels under EOF loading at elevated temperatures. The numerical study was conducted to investigate the impact of web hole size and high temperatures on the web crippling strength and behavior of CHS channels. In addition, the design standards were evaluated by comparing the values of design strengths to the web crippling strength of channels from this study. Using the FEA results, new reliable design equations were recommended to consider the web crippling strength reduction factor of CHS perforated channels at elevated temperatures.

2. Web Crippling Failure

The adoption of cold-formed structural elements in low to mid-rise structures incurs these members to concentrated loads introduced by transfer structures or irregular framing. Depending on the loading condition, these forces result in different failure modes. The most common failure modes are shear failure, buckling, bending, web crippling, or a combination of different modes [27]. As shown in Figure 1, a localised failure of the web beneath the bearing stress is presented as web crippling failure.

2.1. End-One-Flange Loading

The cold-formed beams are often subjected to various web crippling failures, depending on the location of the loads. Four types of failure load cases are available in Figure 2. Only the EOF load case was considered among these loadings in this study.

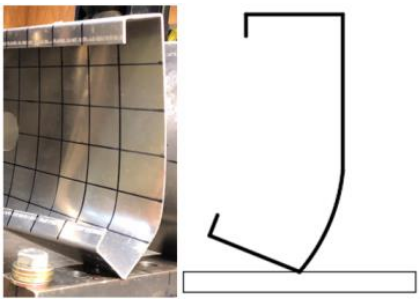

Figure 1. Web crippling failure at a reaction point.

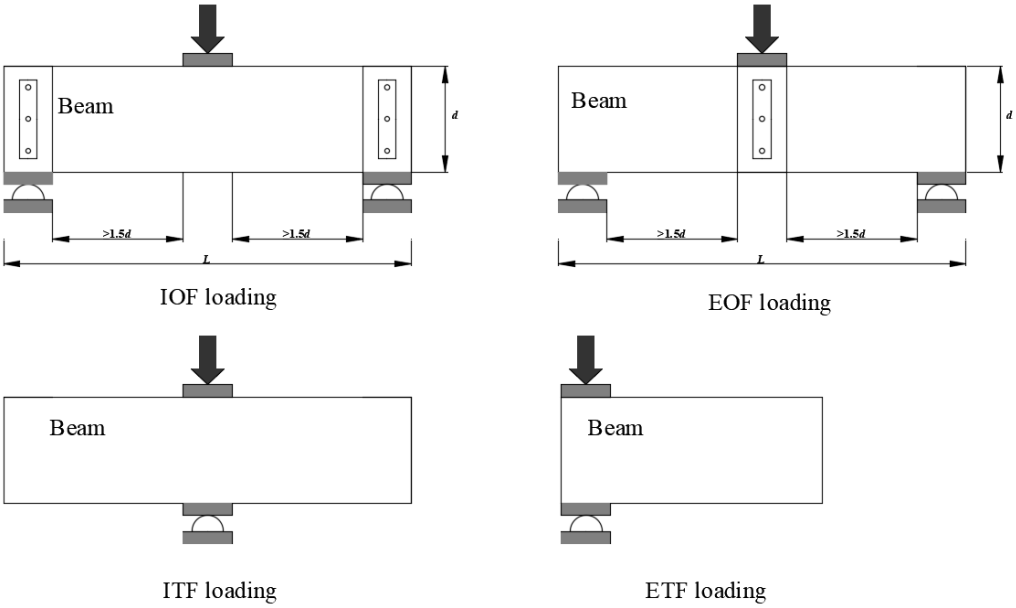

Figure 2. Four loading cases for web crippling tests.

2.2. Experimental Investigation

Lian et al. [15] and Sundararajah et al. [28] conducted experiments on cold-formed structural members subjected to EOF loading. The size and position of web holes were altered to examine their effects on the web crippling strength of channel sections. The specimens were collected with the web holes centered and offset with respect to the bearing plates. Variables such as nominal thickness, web depth, flange width, and web slenderness (h/t) were evaluated on three distinct cross sections.

2.3. Current Design Codes

The AS/NZS [10] and AISI [26] both include the web crippling strength prediction equation. Equation (1) is provided to calculate the nominal web crippling strength per web ($P_{AISI\&AS/NZS}$) for a channel segment without web holes.

$$P_{AISI\&AS/NZS} = Ct_w^2 f_y sin(\theta)\left(1 - C_r\sqrt{\frac{r_i}{t_w}}\right)\left(1 + C_l\sqrt{\frac{N}{t_w}}\right)\left(1 - C_w\sqrt{\frac{h}{t_w}}\right) \quad (1)$$

where, f_y refers to yield stress of channel section; C refers to coefficient; r_i is the inside bent radius; t_w defines the thickness of web; θ is angle between the plane of the web and bearing surface planes, which is equal to 90°; C_r refers to coefficient of inside bent radius; C_l refers to coefficient of bearing; C_w refers to coefficient of web slenderness; N refers to actual bearing length; h is the depth of flat portion of the web; coefficients of C, C_r, C_l, and C_w, for fastened flanges and un-fastened flanges are given in Table 1.

Table 1. Coefficients for fastened and un-fastened channels under EOF load case [10].

	C	C_r	C_l	C_w
Un-fastened	4.0	0.40	0.60	0.03
Fastened	4.0	0.14	0.35	0.02

A reduction factor ($R_{AISI\&AS/NZS}$) is provided to calculate the reduced web crippling strength of CFS channels with web openings. The reduction factor (R) for EOF loading, when the web openings are away from the bearing length, can be calculated using the following equation:

$$R_{AISI\&AS/NZS} = 1.01 - 0.325\frac{a}{h} + 0.083\frac{x}{h} \leq 1 \quad (2)$$

where a refers to web hole diameter; h refers to depth of web flat region; x refers to distance between bearing edge (nearest) and web opening.

3. Numerical Simulation

3.1. General

The non-linear FE models for unfastened and fastened CHS channels were developed using ABAQUS [29]. The centerline dimensions of the CHS channel section were considered. The model was developed using cross-sectional dimensions. As shown in Figure 3, four parts were defined to simulate the testing configuration, namely the channel section, the support bearing plates placed at both ends of the channel section, and the supporting block fastened at the back of the channel section using connectors. The section web crippling associated capacity was obtained by picking up the reaction forces through the support-bearing plates. Figure 4 summarizes the CHS channel symbol definitions, where the labelling of the specimen is shown in Figure 5. The detailed modelling technique is described below.

3.2. Material Property

The stress-strain curve for steel grade S690QL at ambient and elevated temperatures was taken from the study of Winful et al. [30]. It was then transformed to actual stress-plastic strain using Equations (3) and (4) [29]. The stress-strain material curves are shown in Figure 6 and the material properties of S690QL steel grade are summarised in Table 2.

$$\sigma_{true} = \sigma(1 + \varepsilon) \quad (3)$$

$$\varepsilon_{true(pl)} = ln(1 + \varepsilon) - \frac{\sigma_{true}}{E} \quad (4)$$

where E refers to Young's modulus, σ_{true} refers to the true stress, $\varepsilon_{true(pl)}$ refers to the plastic strain, σ and ε are the engineering stress and strain, respectively.

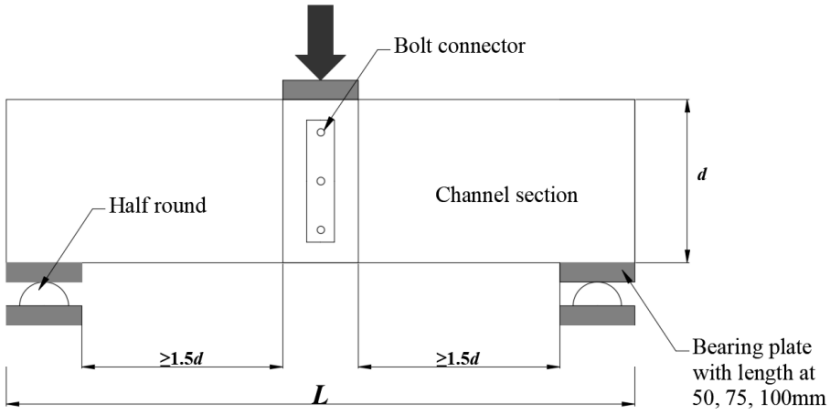

Figure 3. Test configuration.

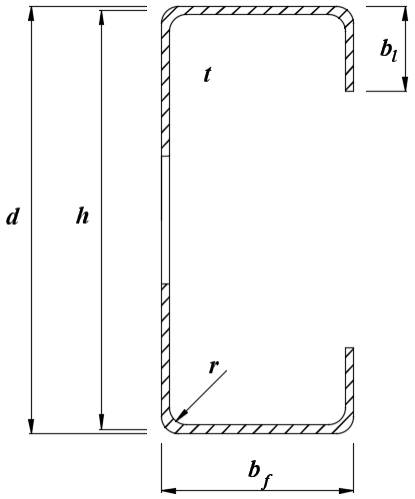

Figure 4. Definition of symbols from the published experiments.

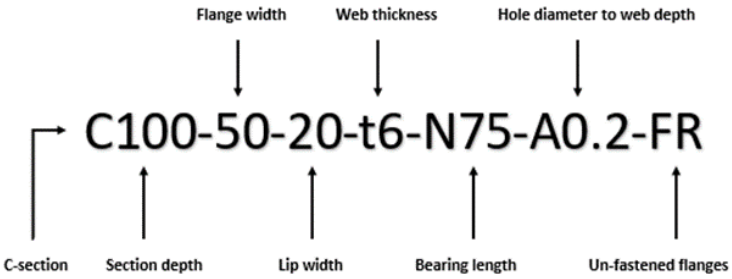

Figure 5. Specimen labelling.

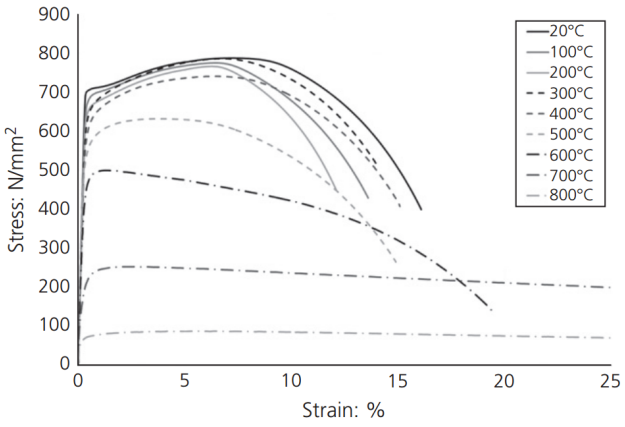

(**a**) up to 25% strain

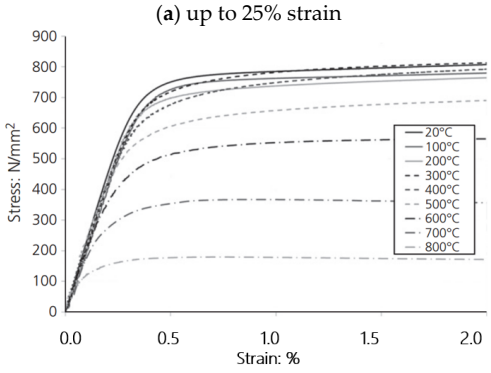

(**b**) up to 2% strain

Figure 6. Engineering stress-strain curves for steel S690QL from 20 to 800 °C from Winful et al. [30].

Table 2. Material properties of CFS S690QL steel grade [30].

Temperature (°C)	f_y (MPa)	E (MPa)
20	739.3	199,300
200	702.335	191,328
400	687.549	177,377
600	487.938	149,475
800	81.323	53,811

3.3. Meshing and Element Type

For a modelling element type consistent with previous researchers [15–22,31–34], a quadrilateral shell SR4 element type with four nodes was used to model channels in ABAQUS, which is applicable for general shell purpose application and can capture finite membrane shell strains that are suitable for structural analysis. A mesh size (5 mm × 5 mm) was adopted for the channels, where a mesh convergence setting is ensured in the analysis acceptance criteria. The mesh size of 10 mm × 10 mm was adequate for the bearing plates. For validating the FE model, smaller mesh sizes were adopted at the inside bend corners and around the web openings. The mesh sizes for different parts are shown in Figure 7 for FE models.

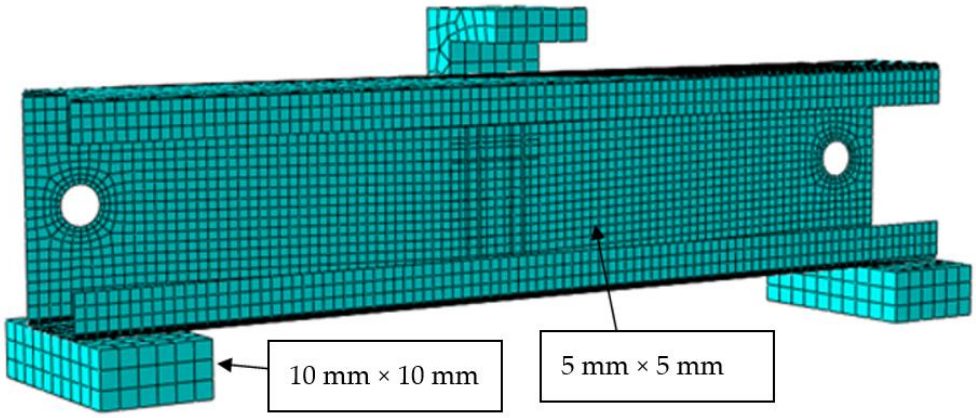

Figure 7. Meshing type in FE models.

3.4. Loading and Boundary Conditions

The Surface-to-Surface contact feature in the ABAQUS interaction library was adopted to simulate the contact between the support-loading plates and the CHS channels. A friction coefficient of 0.4 was employed between the channels and the support-bearing plates. The contact interfaces were constrained not to allow penetrating surfaces into each other. For models with fastened flange, connectors were used to generate the fastened condition for the support bearing plates on the channels. The bearing plates with a roller support condition shown in Figure 3 were modelled by restraining the nodes along the support bearing in translation. The reaction forces were collected using the same node set. The top bearing plate was unfastened in the vertical direction, while other directions were fastened to achieve load-displacement corresponding to the Y-direction in ABAQUS. Figure 8 shows the boundary conditions used in the FE model.

A displacement control method was adopted in this study by applying a vertical load to the top bearing plate attached to the channel section. The nodes of the top bearing plate were bound as a rigid body and connected to a reference point using this procedure. The displacement control was applied to the reference point and displaced vertically (Y-axis) to a predetermined value.

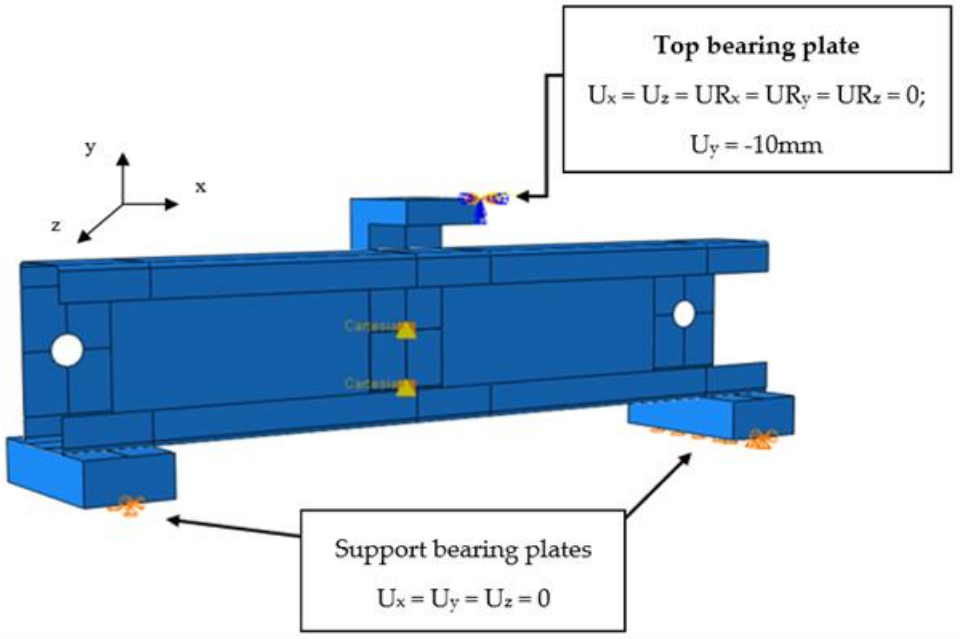

Figure 8. Boundary conditions used in FE models.

3.5. Validation of FE Model

In this study, the developed FE models of the channels under EOF loading were validated using the test data of Lian et al. [15] and Sundararajah et al. [28]. Due to the paucity of data for the perforated CHS channels, the validation study against Lian et al. [15] and Sundararajah et al. [28] experimental tests were limited to the CFS channels only. The results of a comparison between the FEA-obtained web crippling strength and the experimental test [28] are shown in Table 3. The mean and coefficient of variation (COV) of experimental to FEA results (P_{EXP}/P_{FEA}) are 1.02 and 0.07 for the unfastened channel and 1.03 and 0.04 for the fastened channel, showing adequate accuracy for the parametric study. The FE model can calculate the web crippling strength of CHS channels subjected to EOF loading at room temperature, as concluded.

Table 3. Comparison of FEA results with the experimental investigations from Lian et al. [15] and Sundararajah et al. [28].

Specimen ID	Web	Flange	Lip	Bend Radius	Thickness	Hole Dia	Bearing Length	Yield Stress	Exp.Load	FEA Result	P_{EXP}/P_{FEA}
	d	b_f	b_l	r	t	a	N	f_y	P_{EXP}	P_{FEA}	
	(mm)	(mm)	(mm)	(mm)	(mm)	(mm)	(mm)	(MPa)	(kN)	(kN)	
Sections with un-fastened flanges											
1	101	50.4	14.5	3.5	1.03	0	25	581	3.92	4.17	0.94
2	101	51.1	15.6	4	1.52	0	50	540	9.62	10.29	0.93
3	151.4	61.3	19.6	4.5	1.52	0	50	531	8.75	8.98	0.97
4	203.4	76.4	19.8	5	1.91	0	100	506	12.39	11.16	1.11
5	203.8	77.7	22	5	2.41	0	100	526	20.05	22.83	0.88
6	142.7	59.79	13.23	4.8	1.23	0	100	639.8	4.78	4.34	1.10
7	142.09	60.07	13.34	4.8	1.25	0	120	639.8	5.41	4.77	1.13
8	142.22	60.03	13.11	4.8	1.23	55.17	120	639.8	4.66	4.32	1.08
9	142.27	60	13.26	4.8	1.25	55.27	120	639.8	4.22	4.13	1.02
10	142.15	60.06	13.27	4.8	1.24	0	150	639.8	5.56	5.03	1.11
11	142.17	60	13.16	4.8	1.23	55.11	150	639.8	5.00	4.66	1.07
12	202.07	65.37	14.85	5	1.35	0	120	649.6	4.60	4.31	1.07
13	202.02	65.42	14.75	5	1.35	79.34	120	649.6	3.89	4.23	0.92

Table 3. *Cont.*

Specimen ID	Web	Flange	Lip	Bend Radius	Thickness	Hole Dia	Bearing Length	Yield Stress	Exp.Load	FEA Result	P_{EXP}/P_{FEA}
	d	b_f	b_l	r	t	a	N	f_y	P_{EXP}	P_{FEA}	
	(mm)	(mm)	(mm)	(mm)	(mm)	(mm)	(mm)	(MPa)	(kN)	(kN)	
Sections with un-fastened flanges											
14	202.13	65.4	14.72	5	1.35	0	150	649.6	4.96	4.81	1.03
15	202.05	65.22	14.87	5	1.35	79.4	150	649.6	4.37	4.33	1.01
16	202.41	65.26	14.31	5	1.35	99.52	150	649.6	3.85	3.95	0.97
17	303.42	88.2	18.56	5	1.9	0	100	670.6	7.92	7.50	1.06
18	303.04	88.15	18.67	5	1.9	179.07	100	670.6	6.80	6.40	1.06
19	302.35	89.08	18.61	5	1.9	0	120	670.6	8.66	7.77	1.11
20	303.63	89.3	18.62	5	1.9	89.58	120	670.6	8.62	9.49	0.91
21	303.37	88.86	18.45	5	1.9	0	150	670.6	8.81	8.10	1.09
22	303.47	89.73	18.38	5	1.9	119.28	150	670.6	8.30	8.57	0.97
Average											1.02
Cov											0.07
Sections with fastened flanges											
23	142.13	60.06	13.17	4.8	1.27	0	100	639.8	7.07	6.98	1.01
24	142.06	60.02	13.06	4.8	1.27	55.27	100	639.8	6.79	6.64	1.02
25	142.18	60.11	13.22	4.8	1.25	55.18	100	639.8	5.68	6.18	0.92
26	142.17	60.13	13.11	4.8	1.24	55.29	120	639.8	7.08	6.81	1.04
27	142.27	59.99	13.14	4.8	1.23	0	150	639.8	7.97	7.79	1.02
28	142.26	60.09	13.21	4.8	1.23	55.25	150	639.8	7.24	7.46	0.97
29	202.01	65.57	14.51	5	1.35	0	100	649.6	6.53	6.36	1.03
30	202.01	65.22	14.86	5	1.35	79.34	100	649.6	6.39	6.02	1.06
31	202.02	65.39	14.71	5	1.35	0	120	649.6	7.11	6.74	1.05
32	202	65.43	14.84	5	1.35	79.34	120	649.6	6.61	6.41	1.03
33	201.6	65.46	14.24	5	1.33	99.5	120	649.6	5.98	5.93	1.01
34	202.01	65.45	14.75	5	1.32	0	150	649.6	7.73	6.95	1.11
35	202.03	65.18	14.77	5	1.33	79.37	150	649.6	7.12	6.73	1.06
36	202.43	65.42	14.36	5	1.34	99.57	150	649.6	6.80	6.59	1.03
Average											1.03
Cov											0.04

In this study, it was assumed that the modelling procedure for CHS channels with and without web holes under EOF loading case at elevated temperature was the same as at ambient temperature, and the material properties were modified to account for the lower yield stress and other material properties at elevated temperature.

Using validated FE models, the FEA results from selected models (shown in Table 4) were compared to the predicted web crippling strength determined by AISI and AS/NZS standards [10,26]. Table 5 reveals that the FEA results closely matched to the calculation results determined by design standards.

Table 4. Geometric properties of FE models of channel sections with web openings.

Specimen	h (mm)	b_f (mm)	b_l (mm)	r_i (mm)	t_w (mm)	a (mm)	N (mm)	L (mm)
C100-50-20-t2.5-N50-A0-FR	91.5	50	20	3	2.5	0.0	50	474.5
C100-50-20-t2.5-N50-A0.2-FR	91.5	50	20	3	2.5	18.3	50	474.5
C100-50-20-t2.5-N50-A0.4-FR	91.5	50	20	3	2.5	36.6	50	474.5
C100-50-20-t2.5-N50-A0.6-FR	91.5	50	20	3	2.5	54.9	50	474.5
C100-50-20-t2.5-N50-A0.8-FR	91.5	50	20	3	2.5	73.2	50	474.5
C150-50-20-t2.5-N50-A0-FR	141.5	50	20	3	2.5	0.0	50	624.5

Table 4. *Cont.*

Specimen	h (mm)	b_f (mm)	b_l (mm)	r_i (mm)	t_w (mm)	a (mm)	N (mm)	L (mm)
C150-50-20-t2.5-N50-A0.2-FR	141.5	50	20	3	2.5	28.3	50	624.5
C150-50-20-t2.5-N50-A0.4-FR	141.5	50	20	3	2.5	56.6	50	624.5
C150-50-20-t2.5-N50-A0.6-FR	141.5	50	20	3	2.5	84.9	50	624.5
C150-50-20-t2.5-N50-A0.8-FR	141.5	50	20	3	2.5	113.2	50	624.5
C200-50-20-t2.5-N50-A0-FR	191.5	50	20	3	2.5	0.0	50	774.5
C200-50-20-t2.5-N50-A0.2-FR	191.5	50	20	3	2.5	38.3	50	774.5
C200-50-20-t2.5-N50-A0.4-FR	191.5	50	20	3	2.5	76.6	50	774.5
C200-50-20-t2.5-N50-A0.6-FR	191.5	50	20	3	2.5	114.9	50	774.5
C200-50-20-t2.5-N50-A0.8-FR	191.5	50	20	3	2.5	153.2	50	774.5

Table 5. Comparison of FEA results with current design standards.

Specimen	Ultimate Web Crippling Strength per Web (kN)		Comparison
	P_{FEA}	$P_{ASISI\&AS/NZS}$	$P_{FEA}/P_{AISI\&AS/NZS}$
C100-50-20-t2.5-N50-A0-FR	38.61	31.30	1.22
C100-50-20-t2.5-N50-A0.2-FR	38.49	30.46	1.26
C100-50-20-t2.5-N50-A0.4-FR	37.50	29.30	1.22
C100-50-20-t2.5-N50-A0.6-FR	34.59	27.00	1.25
C100-50-20-t2.5-N50-A0.8-FR	27.48	24.71	1.11
C150-50-20-t2.5-N50-A0-FR	29.85	29.61	1.00
C150-50-20-t2.5-N50-A0.2-FR	29.17	28.78	1.01
C150-50-20-t2.5-N50-A0.4-FR	27.29	26.87	1.02
C150-50-20-t2.5-N50-A0.6-FR	24.89	24.87	1.00
C150-50-20-t2.5-N50-A0.8-FR	23.47	23.14	1.01
C200-50-20-t2.5-N50-A0-FR	23.73	28.20	0.84
C200-50-20-t2.5-N50-A0.2-FR	23.20	27.49	0.84
C200-50-20-t2.5-N50-A0.4-FR	21.43	25.57	0.83
C200-50-20-t2.5-N50-A0.6-FR	19.74	24.03	0.82
C200-50-20-t2.5-N50-A0.8-FR	16.53	21.81	0.76
Average			1.01
COV			0.16

4. Parametric Study

Using validated FE models, a comprehensive parametric investigation has been conducted to examine the effects of increasing temperature on the web crippling strength of CHS channels under EOF loading and associated strength reductions due to web holes. The objective of the parametric research is to determine the qualitative effect of parameter changes on the web crippling strength of CHS using the existing database. These parameters would be included into the proposed equation in the subsequent section. In total, there were 1710 FEA models generated and assessed. Web depth (b_w) ranged from 100 to 300 mm; diameter of web opening to the height of web (a/h) ranged from 0.2 to 0.8; length of bearing plate to the height of web (N/h) ranged from 0.17 to 1.14; and section thickness (t_w) ranged from 2, 4, and 6 mm. In addition, various bearing plate lengths (N) were

employed including 50, 75, and 100 mm. The steel grade S690QL was employed with an elastic-perfectly plastic material description based on the material parameters from Table 2.

The strength of CHS channels under EOF loading case is affected by three ratios, namely: r/t, N/t and h/t which correspond to the interior radius to the section thickness, the ratio of bearing length to web thickness and the ratio of web height to its thickness, respectively. The web crippling strength of CHS channels is calibrated by the reduction factor (R). The parametric study only looked at the web crippling strength and behavior of CHS channels containing web holes under EOF loading at elevated temperatures.

The effects of each of these parameters at elevated temperatures are elaborated in the following sections with five temperature levels considered, 20 °C, 200 °C, 400 °C, 600 °C, and 800 °C.

4.1. Parametric Study

4.1.1. Effect of the r/t (Corner Radius/Section Thickness) Ratio on the Web Crippling Strength

The effect of the r/t ratio on the web crippling strength of CHS channels was investigated. As demonstrated in Figure 9, the negative influence of the r/t ratio on the web crippling strength can be observed. At ambient temperature, the average web crippling strength of CHS fastened and unfastened channels fell by 85.77% and 82.45%, respectively, from 0.5 to 1.5.

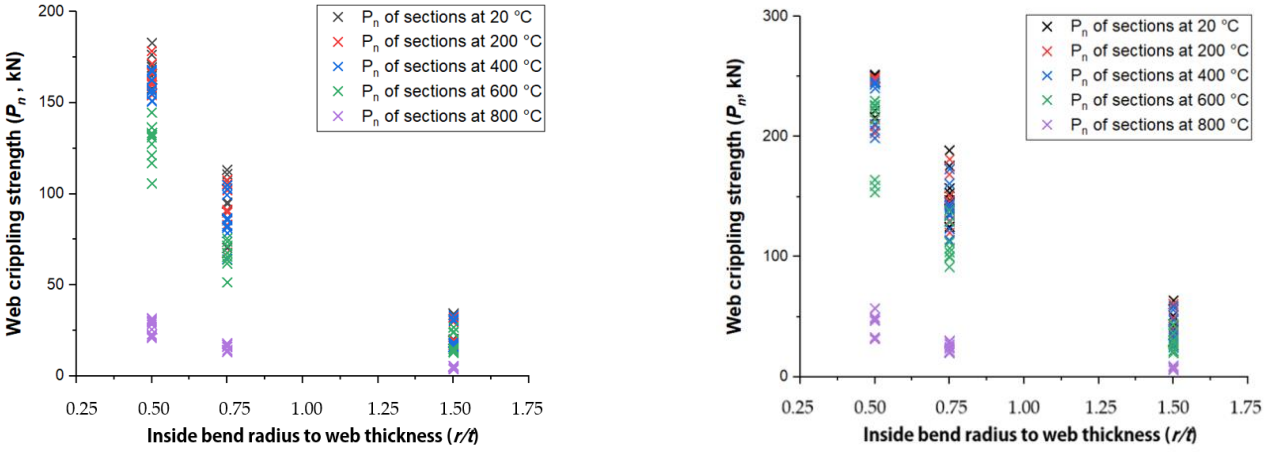

(**a**) Channel sections with unfastened flanges (**b**) Channel sections with fastened flanges

Figure 9. Ratio of r/t against web crippling strength.

4.1.2. Effect of the N/t (Bearing Length/Section Thickness) Ratio on the Web Crippling Strength

Figure 10 shows that the web crippling strength decreases with higher values of N/t ratio from 8 to 50. The average reduced percentages for channel flanges (fastened and unfastened) at ambient temperature are 85.74% and 81.28%, respectively. Upon N/t reaching 37.5, the web crippling strength stabilises at ambient and elevated temperatures.

4.1.3. Effect of the h/t (Web Depth/Section Thickness) Ratio on the Web Crippling Strength

The ratio of the h/t ratio on the web crippling strength is explored as depicted in Figure 11. The rise in the ratio is associated with a reduction in the web crippling strength. The average ultimate web crippling strength of CHS unfastened and fastened channels with unfastened and fastened condition on flanges are lowered by 88.94 % and 86.85 %, respectively, when the h/t ratio is changed from 14.67 to 146.

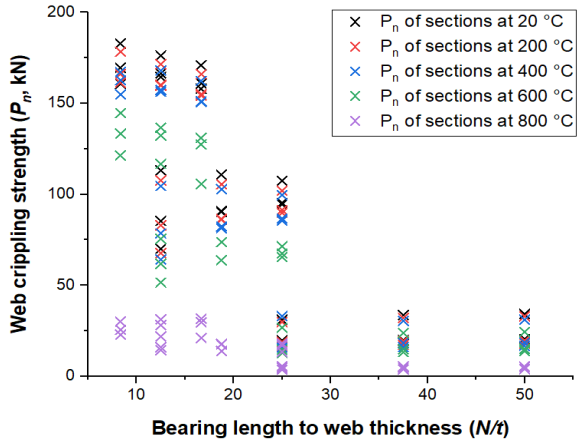

(**a**) Channel sections with unfastened flanges

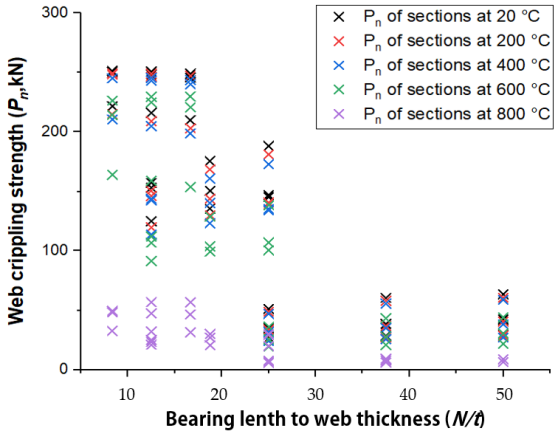

(**b**) Channel sections with fastened flanges

Figure 10. Ratio of N/t against web crippling strength.

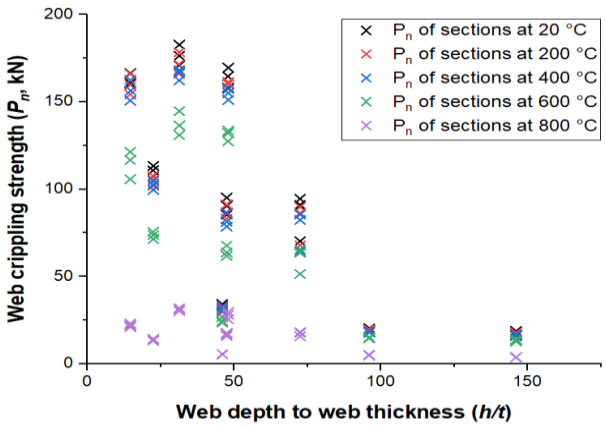

(**a**) Channel sections with un-fastened flanges

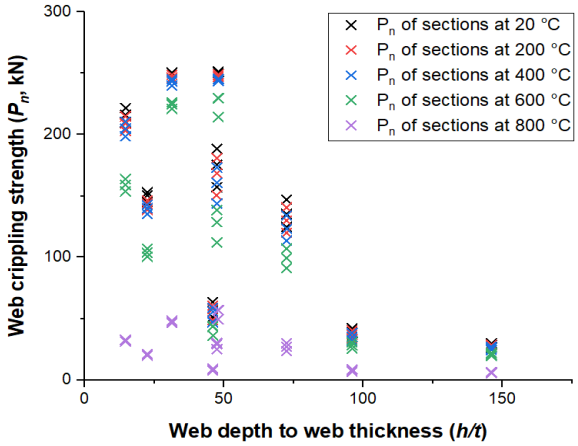

(**b**) Channel sections with fastened flanges

Figure 11. Ratio of h/t against web crippling strength.

4.1.4. Effect of Fastened Flanges on the Web Crippling Strength

From Figure 12, the average ultimate web crippling strength of CHS channels with fastened flange is 28.77 % more than that of CHS channels with unfastened flange. For CHS channels with web holes, the fastened flange condition may prevent the rotation of the flanges, which increases the web crippling strength of such channels under EOF loading.

4.1.5. Effect of Elevated Temperatures on the Web Crippling Strength

Figure 13 shows the web crippling strength of CHS channels response to a temperature gradient. The ultimate web crippling strength decreases as the temperature rises from 20 to 800 °C. As shown in Table 6, the drop percentage in the web crippling strength for unfastened-flange channels is larger than that for fastened-flange channels. Figure 14 depicts some selected failure modes using the Von Mises stress criterion. From Figure 14, it is observed that the out-of-plane deformation of the webs occurs under EOF loading. The failure modes are similar for most of the sections at ambient and high temperatures. However, the stress distribution near the web holes increases as temperature increases (see Figure 14). Furthermore, it was found that the web crippling strength of CHS channels decreases with increasing temperatures.

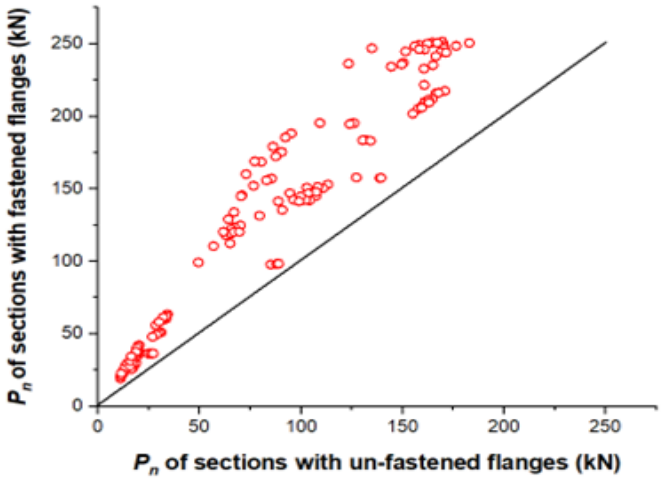

Figure 12. Comparison of web crippling strength of unfastened and fastened flanges.

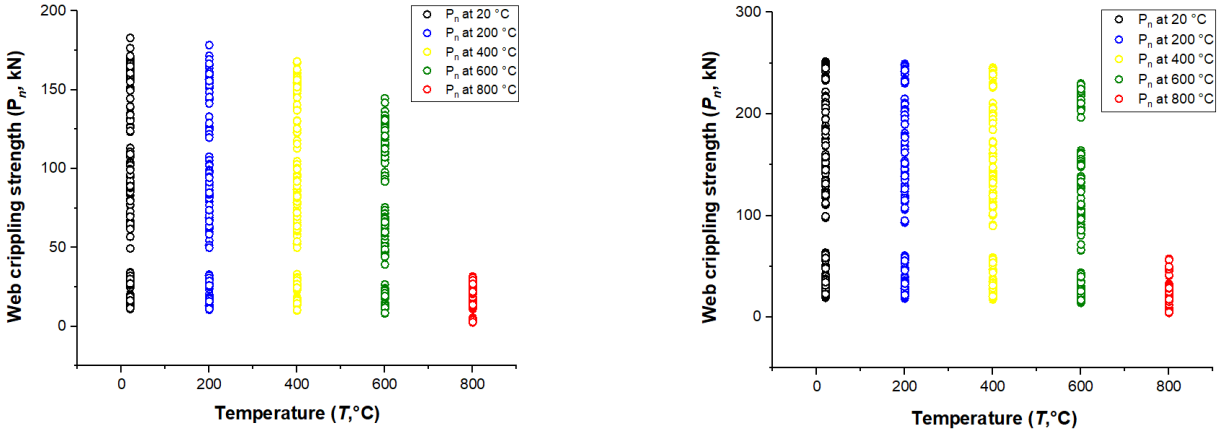

(**a**) Channel sections with unfastened flanges (**b**) Channel sections with fastened flanges

Figure 13. Web crippling strength against temperatures.

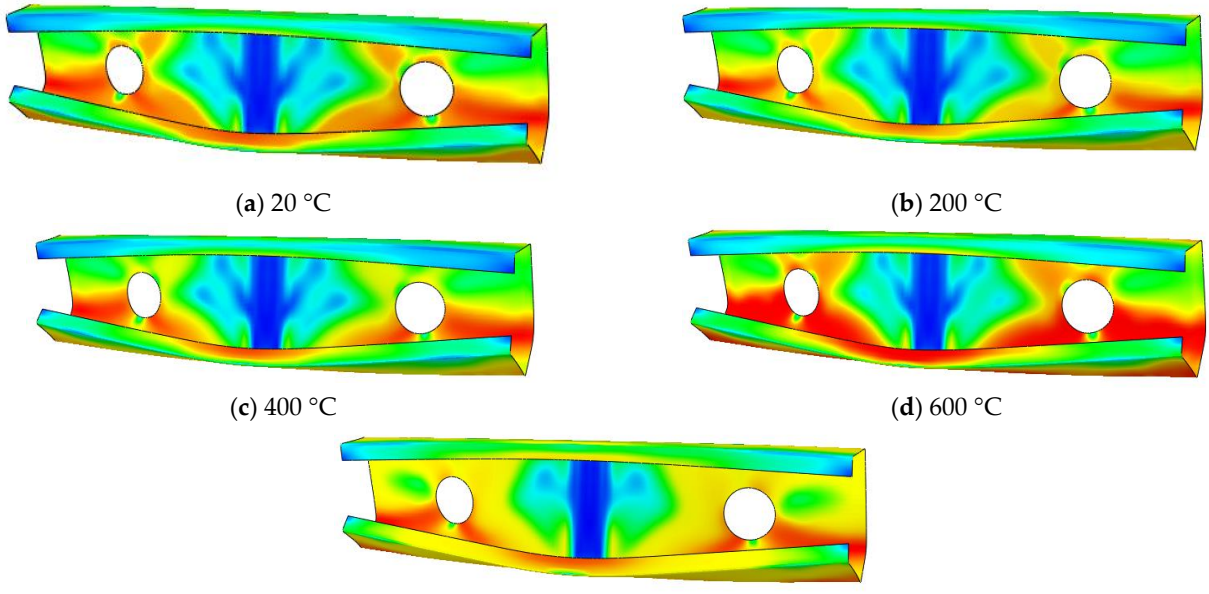

(**a**) 20 °C (**b**) 200 °C

(**c**) 400 °C (**d**) 600 °C

(**e**) 800 °C

Figure 14. Failure modes of specimen C150-50-20-t2.5-N50-A0.4-FR under different temperatures.

Table 6. Average strength reduction percentage (%) of investigated sections at elevated temperature against ambient temperature (T = 20 °C).

		UnFastened Flanges	Fastened Flanges
Temperature	T = 20 °C	–	–
	T = 200 °C	3.66	2.93
	T = 400 °C	6.79	5.72
	T = 600 °C	26.49	22.46
	T = 800 °C	83.10	82.89

4.2. Web Crippling Strength Reduction Factor (R)

Equation (5) provided the web crippling strength reduction factor (R) calculation formula:

$$R = P_{hole}/P_{A0} \quad (5)$$

where P_{hole} is the web crippling strength of section with centered web holes; P_{A0} is the web crippling strength of section without web holes.

4.2.1. Effect of the a/h (Hole Diameter/Web Depth) Ratio on R

Figure 15 and Table 7 illustrate the relationship between the a/h ratio and the web crippling strength reduction factor (R). Figure 15 depicts a decreasing trend in the R as a result of the increasing a/h ratio. When the a/h ratio grows from 0.2 to 0.6, CHS channels with fastened flanges see a modest variation in the reduction factor when exposed to various temperatures. In Table 7, the average R value for CHS unfastened channels reduces from 0.95 to 0.75, with an increase in a/h ratio. Similarly, the average R value for CHS fastened channels decreases from 0.99 to 0.73.

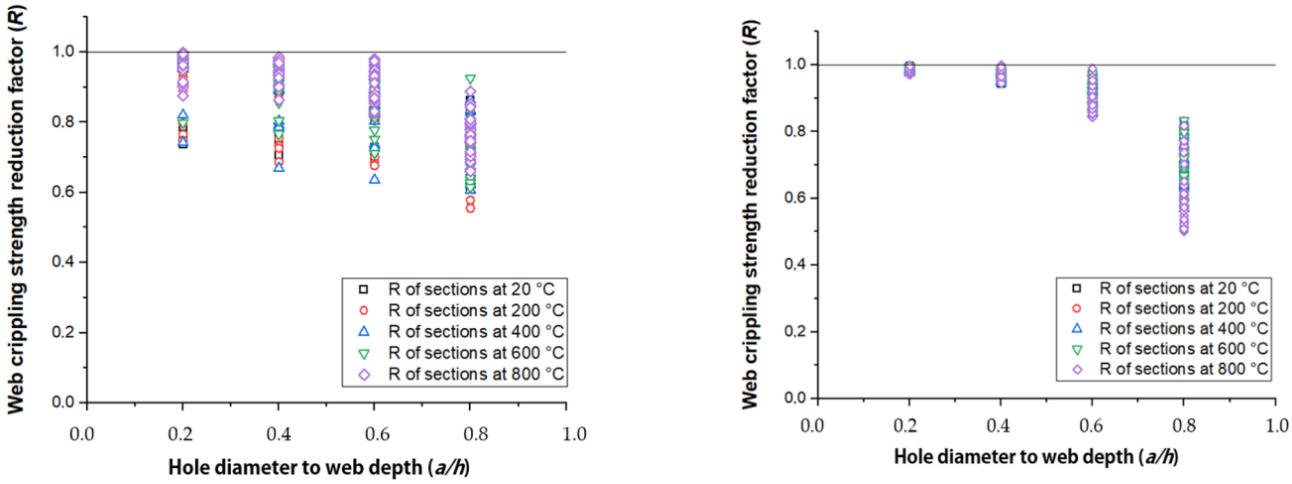

(**a**) Channel sections with unfastened flanges (**b**) Channel sections with fastened flanges

Figure 15. Strength reduction factor against a/h.

Table 7. Average strength reduction factor (R) of investigated sections.

		Unfastened Flanges	Fastened Flanges
a/h	0.2	0.95	0.99
	0.4	0.91	0.97
	0.6	0.85	0.92
	0.8	0.75	0.73

4.2.2. Effect of the N/h (Bearing Length/Web Depth) Ratio on R

The web crippling strength reduction factor (R) for CHS fastened channels has a significant influence with N/h ratio increases and an a/h ratio larger than 0.8. The factor R fluctuates between 1% and 30% when the N/h ratio rises from 0.17 to 1.14 for CHS unfastened channels, depending on the a/h ratio. A ratio of 0.8 a/h corresponds to the steepest decline.

4.2.3. Effect of Fastened Flanges on R

As seen in Figure 15, fastened sections behave more rigidly than unfastened sections when a/h varies between 0 and 0.8, with a little variance of around 4%.

5. Proposed Design Equations

Since existing design standards do not effectively predict the web crippling strength of CHS channels at elevated temperatures, the FEA parametric results were utilized to propose new equations to address this issue. Using SPSS analytical software [35], a statistical analysis was undertaken to propose a design equation including results from the parametric results of this study. The proposed equation has the following limits: $r/t \leq 1.5$, $N/t \leq 50$, $h/t \leq 146$, $a/h \leq 0.8$, $N/h \leq 1.14$.

Equation (6) represents the design equation to determine the web crippling strength reduction factors (R_{prop}) of CHS channels with centered web holes:

$$R_{prop} = \alpha - \gamma \frac{a}{h} + \lambda \frac{N}{h} \quad (6)$$

$$R = P_w / P_0 \quad (7)$$

where α, γ, and λ are coefficients, and α, γ, and λ values obtained with SPSS are given in Table 8. P_w is the web crippling strength of the perforated channel section, and P_0 is the web crippling strength of the unperforated same channel section.

Table 8. Proposed equation coefficients for reduction factor (R).

Coefficient	Flanges Unfastened to Support	Flanges Fastened to Support
α	0.961	1.115
γ	0.317	0.411
λ	0.120	−0.017

To quantify the accuracy of the proposed equations, a comparison was conducted between the results from the equations and the FEA results as well as between design codes. Using the FEA data, Equation (6) was utilised to calculate the reduction factors for EOF web crippling strength. Tables 9 and 10 demonstrate that the recommended web crippling strength reduction factors (R_{prop}) estimate the reduction in ultimate failure strength of CHS channels with web holes under EOF loading with high accuracy. The average values of the proposed web crippling strength reduction factor R/R_{prop} ratio are less than the factors provided by the AISI and AS/NZS design standard ($R/R_{\text{AISI\&AS/NZS}}$) and have a smaller coefficient of variation (COVs) showing better accuracy and prediction. It also can be seen from Table 10 that the COVs derived from the proposed equations and AISI and AS/NZS [10,26] are comparable when compared to CHS fastened channels.

Table 9. Comparison of proposed equations for strength reduction factor with other calculation methods for channel sections with unfastened flanges.

Specimen	Failure Load without Web Holes	Reduction Factors			$R/R_{AISI\&AS/NZS}$	R/R_{prop}
	P_0 (kN)	$R = P_w/P_0$	$R_{AISI\&AS/NZS}$	R_{prop}		
Channel sections at 20 °C						
C100-50-20-t6-N75-A0.2-FR	166.50	0.99	0.97	0.99	1.02	0.99
C100-50-20-t6-N75-A0.4-FR	166.50	0.98	0.90	0.94	1.09	1.04
C100-50-20-t6-N75-A0.6-FR	166.50	0.96	0.82	0.87	1.16	1.10
C100-50-20-t6-N75-A0.8-FR	166.50	0.84	0.75	0.81	1.12	1.04
Average					1.10	1.04
COV					0.05	0.04
Channel sections at 200 °C						
C100-50-20-t6-N75-A0.2-FR	159.74	0.99	0.97	0.99	1.02	0.99
C100-50-20-t6-N75-A0.4-FR	159.74	0.98	0.90	0.94	1.09	1.04
C100-50-20-t6-N75-A0.6-FR	159.74	0.96	0.82	0.87	1.16	1.10
C100-50-20-t6-N75-A0.8-FR	159.74	0.78	0.75	0.81	1.04	0.96
Average					1.08	1.02
COV					0.06	0.06
Channel sections at 400 °C						
C100-50-20-t6-N75-A0.2-FR	156.39	0.99	0.97	0.99	1.02	0.99
C100-50-20-t6-N75-A0.4-FR	156.39	0.97	0.90	0.94	1.08	1.03
C100-50-20-t6-N75-A0.6-FR	156.39	0.95	0.82	0.87	1.15	1.08
C100-50-20-t6-N75-A0.8-FR	156.39	0.83	0.75	0.81	1.10	1.02
Average					1.09	1.03
COV					0.05	0.04
Channel sections at 600 °C						
C100-50-20-t6-N75-A0.2-FR	116.76	0.98	0.97	0.99	1.01	0.98
C100-50-20-t6-N75-A0.4-FR	116.76	0.96	0.90	0.94	1.07	1.02
C100-50-20-t6-N75-A0.6-FR	116.76	0.94	0.82	0.87	1.14	1.07
C100-50-20-t6-N75-A0.8-FR	116.76	0.79	0.75	0.81	1.05	0.97
Average					1.07	1.01
COV					0.05	0.04
Channel sections at 800 °C						
C100-50-20-t6-N75-A0.2-FR	21.85	0.99	0.97	0.99	1.02	0.99
C100-50-20-t6-N75-A0.4-FR	21.85	0.98	0.90	0.94	1.09	1.05
C100-50-20-t6-N75-A0.6-FR	21.85	0.97	0.82	0.87	1.17	1.11
C100-50-20-t6-N75-A0.8-FR	21.85	0.84	0.75	0.81	1.12	1.04
Average					1.1	1.05
COV					0.06	0.05

Table 10. Comparison of proposed equations for strength reduction factor (R) with other calculation methods for channel sections with fastened flanges.

Specimen	Failure Load without Web Holes	Reduction Factors			$R/R_{AISI\&AS/NZS}$	R/R_{prop}
	P_0 (kN)	$R = P_w/P_0$	$R_{AISI\&AS/NZS}$	R_{prop}		
Channel sections at 20 °C						
C100-50-20-t6-N75-A0.2-FX	216.10	0.98	0.97	0.99	1.01	0.96
C100-50-20-t6-N75-A0.4-FX	216.10	0.98	0.90	0.94	1.09	1.05
C100-50-20-t6-N75-A0.6-FX	216.10	0.95	0.82	0.85	1.15	1.11
C100-50-20-t6-N75-A0.8-FX	216.10	0.73	0.75	0.77	0.97	0.95
Average					1.05	1.02
COV					0.07	0.07
Channel sections at 200 °C						
C100-50-20-t6-N75-A0.2-FX	209.14	0.98	0.97	0.99	1.01	0.96
C100-50-20-t6-N75-A0.4-FX	209.14	0.98	0.90	0.94	1.09	1.05
C100-50-20-t6-N75-A0.6-FX	209.14	0.95	0.82	0.85	1.15	1.11
C100-50-20-t6-N75-A0.8-FX	209.14	0.72	0.75	0.77	0.96	0.93
Average					1.05	1.01
COV					0.08	0.08
Channel sections at 400 °C						
C100-50-20-t6-N75-A0.2-FX	204.90	0.98	0.97	0.99	1.01	0.96
C100-50-20-t6-N75-A0.4-FX	204.90	0.98	0.90	0.94	1.09	1.05
C100-50-20-t6-N75-A0.6-FX	204.90	0.95	0.82	0.85	1.15	1.11
C100-50-20-t6-N75-A0.8-FX	204.90	0.72	0.75	0.77	0.96	0.93
Average					1.05	1.01
COV					0.08	0.08
Channel sections at 600 °C						
C100-50-20-t6-N75-A0.2-FX	158.90	0.98	0.97	0.99	1.01	0.96
C100-50-20-t6-N75-A0.4-FX	158.90	0.98	0.90	0.94	1.09	1.05
C100-50-20-t6-N75-A0.6-FX	158.90	0.95	0.82	0.85	1.15	1.11
C100-50-20-t6-N75-A0.8-FX	158.90	0.69	0.75	0.77	0.92	0.89
Average					1.04	1.00
COV					0.09	0.09
Channel sections at 800 °C						
C100-50-20-t6-N75-A0.2-FX	32.27	0.97	0.97	0.99	0.99	0.95
C100-50-20-t6-N75-A0.4-FX	32.27	0.96	0.90	0.94	1.07	1.02
C100-50-20-t6-N75-A0.6-FX	32.27	0.89	0.82	0.85	1.08	1.04
C100-50-20-t6-N75-A0.8-FX	32.27	0.61	0.75	0.77	0.81	0.79
Average					0.99	0.95
COV					0,13	0.11

6. Conclusions

This paper presents a numerical study on the strength and behavior of EOF web crippling on CHS perforated channels with S690QL steel grade at elevated temperatures.

The non-linear FE models of CHS channels with web holes under EOF loading were generated and validated against experimental test data at ambient temperatures. Then, a comprehensive parametric investigation was performed on the web crippling strength of CHS channels under EOF loading at high temperatures.

- In total, 1710 FEA models were examined on the web crippling strength of CHS channels under EOF loading, including the various effects of a/h, N/h, flange type, and elevated temperatures.
- Both the ratios of a/h and N/h influence the web crippling strength reduction factor, with the ratio of a/h having a significant impact on the factor. Besides, the web crippling strength reduction factor is unaffected by temperatures ranging from 20 to 800 °C.
- Using FEA results, new design equations were created to account for the effects of cross-sectional geometry, bearing plate, flange type, and hole size on the EOF loading of CHS channels at elevated temperatures. The recommended design equations for CHS channels are limited to $r/t \leq 1.5$, $N/t \leq 50$, $h/t \leq 146$, $a/h \leq 0.8$, and $N/h \leq 1.14$.
- The proposed equations were compared to AISI and AS/NZS calculation techniques. In particular, for CHS channels with unfastened flanges, the proposed equations outperformed the AISI and AS/NZS equations, as shown by a comparison with experimental data from the literature.

Author Contributions: Conceptualization, Z.F., D.L.C. and K.R.; methodology, Z.F. and D.L.C.; writing—original draft preparation, Z.F.; writing—review and editing, K.R., A.Y. and Y.A.-R.; supervision, K.R. and J.B.P.L. All authors have read and agreed to the published version of the manuscript.

Funding: This research received no external funding.

Institutional Review Board Statement: Not applicable.

Informed Consent Statement: Not applicable.

Data Availability Statement: The data presented in this paper has been properly cited.

Acknowledgments: We would like to express our gratitude to Franck Mahalatchimy and Hao Liang for their contributions to this paper.

Conflicts of Interest: The authors declare no conflict of interest.

Abbreviations

a	Hole diameter
A_e	Effective sectional area
b_f	Flange width
b_l	Lip width
C	Coefficient
CAE	Computer-aided engineering
CHS	Cold-formed high-strength steel
CFS	Cold-formed steel
C_l	Coefficient bearing length
COV	Coefficient of variation
C_r	Coefficient of inside bent radius
C_w	Coefficient of web slenderness
d	Depth of the web
d_l	Lip downturn width
DSM	Direct strength method
E	Young's modulus
EOF	End-One-Flange
EWM	Effective width method;
$F_{AISI\&AS/NZS}$	Nominal axial capacity from AISI&AS/NZS specifications
FE	Finite element
f_e	Least of elastic flexural, torsional, and flexural-torsional buckling stress

FEA	Finite element analysis
FEM	Finite element model
F_{EXP}	Axial capacity from experimental
F_{FEA}	Axial capacity from FEA
f_n	Buckling stress at critical load
F_n	Axial strength
f_y	Yield stress
h	Depth of the flat portion of the web
L	Length of the section
LPF	Load proportionally factor
N	Bearing length
P_0	Web crippling strength of channel sections without web holes
$P_{AISI\&AS/NZS}$	Nominal web crippling strength per web from AISI&AS/NZS specifications
P_{EV}	Concentrated load in FE model
P_{EXP}	Web crippling strength from experimental
P_{FEA}	Web crippling strength from FEA
P_n	Web crippling strength
P_w	Web crippling strength of channel sections with web holes
R	Web crippling strength reduction factor from FEA
R_{prop}	Proposed web crippling strength reduction factor
r	Inside bend radius
$R_{AISI\&AS/NZS}$	Web crippling strength reduction factor from AISI&AS/NZS specifications
S4R	4-noded doubly curved linear shell elements
t_w	Web thickness
x	Nearest distance between the web hole and the edge of bearing
α, γ, λ	Coefficients from proposed equation
ε	Engineering strain
$\varepsilon_{true(pl)}$	Plastic strain
ε_u	Strain at ultimate tensile strength
λ_c	Non-dimensional slenderness
σ	Engineering stress
$\sigma_{0.2}$	0.2% proof stress
$\sigma_{0.5}$	0.5% proof stress
σ_{true}	True stress
σ_u	Ultimate tensile strength

References

1. Kankanamge, N.D.; Mahendran, M. Mechanical properties of cold-formed steels at elevated temperatures. *Thin-Walled Struct.* **2011**, *49*, 26–44. [CrossRef]
2. Yu, Y.; Lan, L.; Ding, F.; Wang, L. Mechanical properties of hot-rolled and cold-formed steels after exposure to elevated temperature: A review. *Constr. Build. Mater.* **2019**, *213*, 360–376. [CrossRef]
3. Ranawaka, T.; Mahendran, M. Experimental study of the mechanical properties of light gauge cold-formed steels at elevated temperatures. *Fire Saf. J.* **2009**, *44*, 219–229. [CrossRef]
4. Javed, M.F.; Hafizah, N.; Memon, S.A.; Jameel, M.; Aslam, M. Recent research on cold-formed steel beams and columns subjected to elevated temperature: A review. *Constr. Build. Mater.* **2017**, *144*, 686–701. [CrossRef]
5. Fang, Z.; Roy, K.; Liang, H.; Poologanathan, K.; Ghosh, K.; Mohamed, A.; Lim, J. Numerical Simulation and Design Recommendations for Web Crippling Strength of Cold-Formed Steel Channels with Web Holes under Interior-One-Flange Loading at Elevated Temperatures. *Buildings* **2021**, *11*, 666. [CrossRef]
6. Fang, Z.; Roy, K.; Lakshmanan, D.; Pranomrum, P.; Li, F.; Lau, H.H.; Lim, J.B. Structural behaviour of back-to-back cold-formed steel channel sections with web openings under axial compression at elevated temperatures. *J. Build. Eng.* **2022**, *54*, 104512. [CrossRef]
7. Gunalan, S.; Bandula Heva, Y.; Mahendran, M. Local buckling studies of cold-formed steel compression members at elevated temperatures. *J. Constr. Steel Res.* **2015**, *108*, 31–45. [CrossRef]
8. Chen, J.; Young, B. Cold-formed steel lipped channel columns at elevated temperatures. *Eng. Struct.* **2007**, *29*, 2445–2456. [CrossRef]
9. Gunalan, S.; Heva, Y.B.; Mahendran, M. Flexural–torsional buckling behaviour and design of cold-formed steel compression members at elevated temperatures. *Eng. Struct.* **2014**, *79*, 149–168. [CrossRef]
10. *AS/NZS 4600:2018*; Cold-Formed Steel Structures. Australia/New Zealand Standard: Wellington, New Zealand, 2018.

11. *BS5950*; Structural Use of Steelwork in Building—Formed Thin Gauge Sections Part 5: Code of Practice for Design of Cold. British Standard: London, UK, 1998.
12. *EN 1993-1-2 Eurocode 3*; Design of Steel Structures: General Rules—Structural Fire Design. British Standards Institutions: London, UK, 2005.
13. *EN 1993-1-3 Eurocode 3*; Design of Steel Structures: General Rules—Supplementary Rules for Cold-Formed Members and Sheeting. British Standards Institutions: London, UK, 2005.
14. Rokilan, M.; Mahendran, M. Design of cold-formed steel columns subject to local buckling at elevated temperatures. *J. Constr. Steel Res.* **2021**, *179*, 106539. [CrossRef]
15. Lian, Y.; Uzzaman, A.; Lim, J.B.; Abdelal, G.; Nash, D.; Young, B. Effect of web holes on web crippling strength of cold-formed steel channel sections under end-one-flange loading condition—Part I: Tests and finite element analysis. *Thin-Walled Struct.* **2016**, *107*, 443–452. [CrossRef]
16. Uzzaman, A.; Lim, J.B.; Nash, D.; Rhodes, J.; Young, B. Cold-formed steel sections with web openings subjected to web crippling under two-flange loading conditions—Part I: Tests and finite element analysis. *Thin-Walled Struct.* **2012**, *56*, 38–48. [CrossRef]
17. Uzzaman, A.; Lim, J.B.; Nash, D.; Rhodes, J.; Young, B. Cold-formed steel sections with web openings subjected to web crippling under two-flange loading conditions—Part II: Parametric study and proposed design equations. *Thin-Walled Struct.* **2012**, *56*, 79–87. [CrossRef]
18. Uzzaman, A.; Lim, J.B.; Nash, D.; Rhodes, J.; Young, B. Web crippling behaviour of cold-formed steel channel sections with offset web holes subjected to interior-two-flange loading. *Thin-Walled Struct.* **2012**, *50*, 76–86. [CrossRef]
19. Uzzaman, A.; Lim, J.B.; Nash, D.; Young, B. Effects of edge-stiffened circular holes on the web crippling strength of cold-formed steel channel sections under one-flange loading conditions. *Eng. Struct.* **2017**, *139*, 96–107. [CrossRef]
20. Uzzaman, A.; Lim, J.B.; Nash, D.; Roy, K. Cold-formed steel channel sections under end-two-flange loading condition: Design for edge-stiffened holes, unstiffened holes and plain webs. *Thin-Walled Struct.* **2020**, *147*, 106532. [CrossRef]
21. Uzzaman, A.; Lim, J.B.; Nash, D.; Roy, K. Web crippling behaviour of cold-formed steel channel sections with edge-stiffened and unstiffened circular holes under interior-two-flange loading condition. *Thin-Walled Struct.* **2020**, *154*, 106813. [CrossRef]
22. Chen, B.; Roy, K.; Fang, Z.; Uzzaman, A.; Chi, Y.; Lim, J.B. Web crippling capacity of fastened cold-formed steel channels with edge-stiffened web holes, un-stiffened web holes and plain webs under two-flange loading. *Thin-Walled Struct.* **2021**, *163*, 107666. [CrossRef]
23. Janarthanan, B.; Mahendran, M.; Gunalan, S. Numerical modelling of web crippling failures in cold-formed steel unlipped channel sections. *J. Constr. Steel Res.* **2019**, *158*, 486–501. [CrossRef]
24. Janarthanan, B.; Sundararajah, L.; Mahendran, M.; Keerthan, P.; Gunalan, S. Web crippling behaviour and design of cold-formed steel sections. *Thin-Walled Struct.* **2019**, *140*, 387–403. [CrossRef]
25. Gunalan, S.; Mahendran, M. Web crippling tests of cold-formed steel channels under two flange load cases. *J. Constr. Steel Res.* **2015**, *110*, 1–15. [CrossRef]
26. *AISI S100-16*; North American Specification for the Design of Cold-Formed Steel Structural Members. American Iron and Steel Institute (AISI): Washington, DC, USA, 2016.
27. Macdonald, M.; Heiyantuduwa, M. A design rule for web crippling of cold-formed steel lipped channel beams based on nonlinear FEA. *Thin-Walled Struct.* **2012**, *53*, 123–130. [CrossRef]
28. Sudararajah, L.; Mahendran, M.; Keerthan, P. Web crippling experiments of high strength lipped channel beams under one-flange loading. *J. Constr. Steel Res.* **2017**, *138*, 851–866. [CrossRef]
29. ABAQUS. *Analysis User's Manual, Version 6.14-2*; ABAQUS Inc.: Palo Alto, CA, USA, 2018.
30. Winful, D.A.; Cashell, K.A.; Afshan, S.; Barnes, A.M.; Pargeter, R.J. Elevated temperature material behaviour of high-strength steel. *Proc. Inst. Civ. Eng.-Struct. Build.* **2017**, *170*, 777–787. [CrossRef]
31. Fang, Z.; Roy, K.; Ingham, J.M.; Lim, J.B. Assessment of end-two-flange web crippling strength of roll-formed aluminium alloy perforated channels by experimental testing, numerical simulation, and deep learning. *Eng. Struct.* **2022**, *268*, 114753. [CrossRef]
32. Fang, Z.; Roy, K.; Chi, Y.; Chen, B. Finite element analysis and proposed design rules for cold-formed stainless steel channels with web holes under end-one-flange loading. *Structures* **2021**, *34*, 2876–2899. [CrossRef]
33. Fang, Z.; Roy, K.; Dai, Y.; Lim, J.B. Effect of web perforations on end-two-flange web crippling behaviour of roll-formed aluminium alloy unlipped channels through experimental test, numerical simulation and deep learning. *Thin-Walled Struct.* **2022**, *179*, 109489. [CrossRef]
34. Kanthasamy, E.; Chandramohan, D.L.; Shanmuganathan, G.; Poologanathan, K.; Gatheeshgar, P.; Corradi, M.; Mcintosh, A. Web crippling behaviour of cold-formed high-strength steel unlipped channel beams under End-One-Flange load case. *Case Stud. Constr. Mater.* **2022**, *16*, e01022. [CrossRef]
35. IBM Corp. *IBM SPSS Statistics for Windows, Version 27.0*; IBM Corp.: Armonk, NY, USA, 2020.